Hepatic oleate regulates adipose tissue lipogenesis and fatty acid oxidation[S]

Maggie S. Burhans,* Matthew T. Flowers,† Kristin R. Harrington,† Laura M. Bond,† Chang-An Guo,† Rozalyn M. Anderson,§, and James M. Ntambi[1,*,†]**

Departments of Nutritional Sciences,* Biochemistry,† and Medicine,§ University of Wisconsin-Madison, Madison, WI 53706; and Geriatric Research, Education, and Clinical Center,** Veterans Administration Medical Center, Madison, WI 53705

Abstract Hepatic steatosis is associated with detrimental metabolic phenotypes including enhanced risk for diabetes. Stearoyl-CoA desaturases (SCDs) catalyze the synthesis of MUFAs. In mice, genetic ablation of SCDs reduces hepatic de novo lipogenesis (DNL) and protects against diet-induced hepatic steatosis and adiposity. To understand the mechanism by which hepatic MUFA production influences adipose tissue stores, we created two liver-specific transgenic mouse models in the SCD1 knockout that express either human SCD5 or mouse SCD3, that synthesize oleate and palmitoleate, respectively. We demonstrate that hepatic de novo synthesized oleate, but not palmitoleate, stimulate hepatic lipid accumulation and adiposity, reversing the protective effect of the global SCD1 knockout under lipogenic conditions. Unexpectedly, the accumulation of hepatic lipid occurred without induction of the hepatic DNL program. Changes in hepatic lipid composition were reflected in plasma and in adipose tissue. Importantly, endogenously synthesized hepatic oleate was associated with suppressed DNL and fatty acid oxidation in white adipose tissue. Regression analysis revealed a strong correlation between adipose tissue lipid fuel utilization and hepatic and adipose tissue lipid storage. These data suggest an extrahepatic mechanism where endogenous hepatic oleate regulates lipid homeostasis in adipose tissues.—Burhans, M. S., M. T. Flowers, K. R. Harrington, L. M. Bond, C-A. Guo, R. M. Anderson, and J. M. Ntambi. **Hepatic oleate regulates adipose tissue lipogenesis and fatty acid oxidation. *J. Lipid Res.* 2015.** 56: **304–318.**

Supplementary key words β-oxidation • de novo lipogenesis • fatty acid/desaturases • fatty acid/metabolism • lipids • liver • triglycerides • white adipose tissue

Recently, the prevalence of overweight among all adults in the US was estimated to be nearly 70% (1), and has increased more than 2-fold since 1980 (2). With increased adiposity, lipids accumulate ectopically and are associated with increased risk for detrimental metabolic conditions such as nonalcoholic fatty liver disease, insulin resistance, and hypertriglyceridemia (3–5). The balance of lipid storage between liver and adipose depots may play an important role in disease vulnerability. Fat may be synthesized from dietary carbohydrates via de novo lipogenesis (DNL), or sequestered from circulating lipids. The contribution of hepatic and adipose tissue DNL-derived fat to whole-body adiposity is controversial. While it is considered to be quantitatively minimal by some (6, 7), others have demonstrated that DNL-derived lipids can negatively impact metabolic health and contribute to hepatic steatosis and visceral adiposity in humans (8–10). Of particular importance in the context of whole-body metabolic homeostasis, recent evidence suggests that de novo synthesized fatty acids and lipids serve important signaling and regulatory roles in cellular and systemic metabolism (7, 11).

MUFAs are major components of tissue lipids such as TGs, cholesteryl esters (CEs), and GPs, and high levels of MUFAs are inversely associated with metabolic health. The stearoyl-CoA desaturase (SCD) family of enzymes catalyzes the synthesis of MUFAs by insertion of a *cis* double bond at the Δ9 position of saturated fatty acids. The preferred substrates for SCD-catalyzed reactions are palmitate (16:0) and stearate (18:0), and the major

This work was supported by National Institutes of Health (NIH) Grant R01 DK062388, ADA 7-13-BS-118, and USDA Hatch W2005 (to J.M.N.), and NIH Grant RO1 AG037000 (to R.M.A.). M.S.B was supported by NIH Predoctoral Training Grant T32 DK007665, M.T.F was supported by NIH Postdoctoral Training Grant T32 DK007665 and an American Heart Association postdoctoral fellowship, L.M.B. was supported by NIH National Research Service Award T32 GM07215.

Manuscript received 4 September 2014 and in revised form 30 December 2014.

Published, JLR Papers in Press, January 2, 2015
DOI 10.1194/jlr.M054429

Abbreviations: ASM, acid soluble metabolite; CE, cholesteryl ester; DNL, de novo lipogenesis; GKO, stearoyl-CoA desaturase 1 global knockout; GLC, gas liquid chromatography; GLS5, global knockout liver-specific stearoyl-CoA desaturase 5 transgenic; GLS3, global knockout liver-specific stearoyl-CoA desaturase 3 transgenic; LD, lipogenic diet; LKO, stearoyl-CoA desaturase 1 liver knockout; SCD, stearoyl-CoA desaturase; WAT, white adipose tissue.

[1]To whom correspondence should be addressed.
e-mail: jmntambi@wisc.edu

[S] The online version of this article (available at http://www.jlr.org) contains supplementary data in the form of three figures and nine tables.

products of SCD activity are oleate (18:1n-9) and palmitoleate (16:1n-7). In humans, skeletal muscle *SCD1* mRNA abundance is positively correlated with TG synthesis and negatively correlated with TG oxidation, and there is also a strong positive association between muscle SCD1 activity and BMI (12). Serum TGs are largely hepatic in origin and the desaturation index (18:1n-9/18:0) is used to estimate liver SCD activity. In humans, the serum lipid desaturation index positively correlates with overall TG levels, explaining more than 50% of the variation in serum TG levels among individuals (13). Another study revealed that four single nucleotide polymorphisms in human *SCD1* are associated with improved insulin sensitivity, lower BMI, and reduced abdominal adiposity (14).

There are two models of diet-induced obesity, high-carbohydrate diets that drive DNL and high-fat diets that provide excess exogenous lipid. We previously demonstrated that whole-body or global SCD1 knockout (GKO) mice have increased energy expenditure and are protected from obesity and hepatic steatosis induced by both high-carbohydrate and high-fat diets (15, 16). Mice with deletion of SCD1 in liver only (LKO) exhibit the adiposity and hepatic steatosis phenotypes observed in GKO mice when fed a high-carbohydrate diet. In contrast, high-fat diet-fed LKO mice are not protected from weight gain and hepatic steatosis (16). These data suggest that the phenotypes induced by high-carbohydrate diets are driven by liver metabolic events. Although the hepatic lipogenic program is impaired in LKO mice fed a high-carbohydrate diet, dietary supplementation with oleate restores the molecular changes and related lipid accumulation phenotypes (16). Taken together, this body of past work reveals that hepatic SCD1 mediates the lipogenic effects of a high-carbohydrate diet. However, the question of whether local hepatic synthesis of MUFAs is sufficient to restore the response to a high-carbohydrate diet in GKO mice remains unknown. Furthermore, whether oleate and palmitoleate, the major products of SCD-catalyzed reactions, differentially regulate these metabolic processes has not been directly assessed.

Two SCD isoforms have been identified in humans (SCD1 and SCD5) and four in mice (SCD1–4). While mouse SCD1 is expressed at high levels in adipose tissue and is induced in liver under high-carbohydrate conditions, SCD3 expression is restricted to skin, Harderian gland, and the preputial gland (17–19). We took advantage of the substrate preferences of distinct SCD isoforms to restore oleate (human SCD5) or palmitoleate (mouse SCD3) synthesis in the liver only in GKO mice. We show that in the context of a high-sucrose lipogenic diet (LD), hepatic oleate, but not palmitoleate, synthesis increases hepatic lipid accumulation and adiposity in GKO mice. In addition, hepatic oleate is associated with suppression of DNL and fatty acid oxidation in white adipose tissue (WAT). These data suggest that the unfavorable metabolic effects of LDs are mediated by hepatic oleate, the major product of human SCD5.

METHODS

Animals and diets

Two liver transgenic mouse lines were generated by cloning either the human SCD5 cDNA sequence or the mouse SCD3 cDNA sequence into the pLiv.LE6 vector construct (a kind gift from John Taylor, Gladstone Institute) (20). Mice were backcrossed at least seven generations with C57BL/6 mice to generate SCD5Tg+ and SCD3Tg+ mice. SCD5Tg+ and SCD3Tg+ mice were then crossed with SCD1 GKO mice (in C57BL/6 background) to generate compound heterozygous mice, SCD1+/− carrying one copy of the SCD5 or SCD3 transgene. These compound heterozygous mice were then bred with female SCD1+/− or male SCD1−/− mice to generate SCD5Tg+;SCD1−/− (GLS5) and SCD3Tg+;SCD1−/− (GLS3) mice.

Mice were housed in the University of Wisconsin-Madison Department of Biochemistry animal care facility and maintained on a 12 h light-dark cycle (6:00 PM to 6:00 AM) and had free access to food and water unless specified otherwise. All mice were male and were fed a standard rodent chow diet (Purina 5008) at weaning, and were then either maintained on the chow diet or fed a LD that was high in sucrose and very low in fat (Harlan Teklad TD.03045; 2.5% kcal from fat (corn oil), 76.7% kcal from carbohydrate) for a period of 10 days. The age at LD feeding varied among experiments, from 10 to16 weeks of age, and is described specifically for each figure. Unless noted otherwise, all mice were fasted 4 h and euthanized at the same time of day by isoflurane overdose. Blood was collected via cardiac puncture and tissues were collected. All in vivo experimental animal procedures were approved by the Institutional Animal Care and Use Committee at the University of Wisconsin-Madison.

Lipid extraction and gas chromatography

Liver, adipose tissue, and plasma fatty acid analyses were carried out as previously described (21). Lipids were extracted following a modified Folch method (22). Pentadecanoic acid was added as an internal control of transmethylation efficiency. Neutral lipid species were separated on silica gel-60 TLC plates (EMD Millipore) using a heptane/isopropyl ether/acetic acid (60/40/3) solvent system. TG, CE, FFA, and GP bands were scraped from the plates and lipids were extracted and transmethylated using boron trifluoride in 14% methanol (Sigma). Fatty acid methyl esters were suspended in hexane and analyzed by gas liquid chromatography (GLC). Chromatograms were analyzed using HP ChemStation software. Results were calculated to express fatty acid composition as a percent of total and as concentration of micrograms per milligram tissue or micrograms per 100 μl plasma. Total hepatic oleate and total hepatic palmitoleate levels were calculated based on the sum of the respective fatty acid in TG, CE, FFA, and GP fractions for each animal and expressed as a percentage of the level in WT mice. Total fatty acids in each lipid fraction were calculated based on the sum of the total fatty acid mass (micrograms per milligram of tissue) detected by GLC analysis in each fraction. Heptadecanoic acid, triheptadecanoin, cholesteryl heptadecanoate, or diheptadecanoyl phosphocholine internal standards were used to quantify fatty acids in FFA, TG, CE, and GP fractions, respectively.

Liver histology

Fresh liver tissue was fixed in 10% neutral buffered formalin for 2 days at 4°C and then stored in 70% ethanol at 4°C until sectioning and histological analysis. Oil red O staining was performed on cryosections, as previously described (23). Slides were imaged with a 40× objective in a Leica DM4000B microscope.

Plasma and liver biochemical analyses

Plasma TGs were measured in 5 μl plasma using a colorimetric assay with the Infinity TG reagent (Thermo Scientific). Liver TGs were measured in lipid extract from 10 mg liver tissue using a colorimetric enzymatic assay (Wako Chemicals USA). Blood glucose values were measured using a spectrophotometric glucose oxidase and peroxidase assay, as described previously (16). Plasma insulin (Crystal Chem, #90080), plasma leptin (Millipore, #EZML-82K), and plasma FGF21 (R&D Systems, #MF2100) were all measured by ELISA.

RNA isolation and real-time quantitative PCR

Liver total RNA was isolated with Tri reagent (Molecular Research Center) and WAT total RNA was isolated with an RNeasy lipid tissue mini kit (Qiagen) and treated with Turbo DNase (Ambion). RNA was reverse transcribed with a high capacity cDNA reverse transcription kit (Applied Biosystems). Quantitative real-time PCR was performed using SYBR Green PCR Master Mix (Applied Biosystems) and an ABI 7500 instrument (Applied Biosystems). Relative mRNA expression levels of *SCD5* and *Scd3* were calculated using the comparative C_T method, and normalized to *18S* rRNA. Primer sequences used to detect *SCD5* expression were: forward 5′ GCTGTTTGTTCGCAAGCATCGAGA and reverse 5′ AAAGCACATGAGCACCACGGAGAT. For *Scd3* expression, the primer sequences were forward 5′ CATTGGAGCCGGAGTCCATC and reverse 5′ GCCATGGTGTTGGCAATGAT. Other primer sequences are available upon request.

Microsomal protein and SCD activity assays

Hepatic microsomes were prepared by sequential centrifugation as previously described (21). SCD activity assays were performed using 100 μg liver microsomal protein. Microsomes were incubated in potassium phosphate buffer in the presence of 30 μM stearoyl-CoA and 1 μCi ^{3}H-9,10-stearoyl-CoA (or palmitoyl-CoA and ^{3}H-9,10-palmitoyl-CoA) (American Radiolabeled Chemicals) and NADH for 15 min at 24°C. The reaction was quenched by 6% perchloric acid and unused substrate was adsorbed by activated charcoal (Sigma). Samples were counted in a scintillation counter and results were calculated as ^{3}H disintegrations per minute/100 μg protein and are presented as percent of mean WT activity level.

Immunoblotting

Microsomal protein was used for immunoblot analysis of SCD1 (Santa Cruz Biotechnology, #sc-14720), Hemagglutinin tag for SCD5 and SCD3 transgenic protein (Roche Applied Science, #11867423001), human SCD5, GAPDH (Millipore), and transferrin receptor-1 (TfR1; Invitrogen, #13-6890). Proteins were separated by SDS-PAGE in 8–10% gels. Proteins were transferred to polyvinyl difluoride membrane, incubated with primary antibody overnight, followed by secondary antibody, and visualized using Pierce ECL Western blotting substrate.

In vivo DNL

Mice were fasted for 2 h and then injected intraperitoneally with 50 mCi ^{3}H-H_2O. Mice were euthanized by isoflurane overdose 1 h postinjection. Blood was collected by cardiac puncture to determine specific activity. Approximately 100 mg liver tissue or 10 mg gonadal WAT was saponified in 2.5 M KOH/ethanol for 2.5 h at 75°C. The tissues were neutralized with formic acid and lipids were extracted with hexane. Fatty acids and sterols were separated on TLC with a heptane/isopropyl ether/acetic acid (60/40/3) solvent system. Fatty acid and sterol bands were visualized with iodine vapors, scraped, and counted in a liquid scintillation counter. Results were calculated as micromoles of ^{3}H-H_2O per gram of tissue per hour incorporated into fatty acids or cholesterol (24).

Ex vivo fatty acid oxidation

Mice were fasted for 4 h and euthanized by isoflurane overdose. Liver and gonadal WAT were collected and processed as previously described (25). Tissue homogenates were incubated for 1 h in the presence of 300 μM palmitic acid with 0.4 μCi 1-^{14}C-palmitic acid. Fatty acid oxidation inhibitor rotenone (0.75 μM, Sigma Aldrich) was used as a control. ^{14}C-containing acid soluble metabolites (ASMs) and trapped CO_2 were measured in a liquid scintillation counter. Fatty acid oxidation of the two fractions was calculated by [(disintegrations per minute-blank)/reaction mixture specific activity]/gram of tissue, and the total fatty acid oxidation values reported reflect the sum of the CO_2 and acid-soluble metabolite fractions.

Ex vivo lipolysis

Gonadal fat explants isolated from mice (eight mice per group) were washed with ice-cold PBS and cut into small pieces (~75–150 mg). Fat pads were preincubated for 1 h in 140 μl of DMEM (Life Technologies) containing 2% fatty acid-free serum albumin (Sigma-Aldrich). Subsequently, fat pads were incubated in 250 μl of KRH buffer [125 mM NaCl, 5 mM KCl, 1.8 mM $CaCl_2$, 2.6 mM $MgSO_4$, 5 mM HEPES (pH 7.2)] plus 2% BSA (fatty acid free) for 2 h under agitation at 37°C. Free glycerol content was quantified from supernatants using a free glycerol determination kit (Sigma-Aldrich). Glycerol release from each sample was normalized to the weight of each fat pad.

Glucose tolerance tests

Mice were fasted for 4 h prior to the start of glucose tolerance tests. Intraperitoneal injections of 20% dextrose solution at 2 g/kg body weight were administered. Tail vein blood was used to determine blood glucose concentrations at 0, 30, 60, 90, and 120 min following the glucose dose using a blood glucose meter and test strips (One Touch Ultra, Diabetic Express).

Statistical analyses

Results are expressed as mean ± SEM. Variables that did not have a Gaussian distribution were log transformed prior to ANOVA analyses. Data were analyzed using linear regression analyses and one-way ANOVA with Tukey's post hoc test. Results with a P value <0.05 were considered statistically significant. All statistical analyses were performed using GraphPad Prism 6 (GraphPad Software).

RESULTS

Liver SCD5 and SCD3 transgenic mice in the SCD1 GKO background produce hepatic oleate and palmitoleate, respectively

To determine whether hepatic MUFAs exert differential metabolic effects, we generated mice with constitutive expression of either human *SCD5* or mouse *Scd3* in liver tissue only in a GKO background. These SCD isoforms synthesize oleate (SCD5) and palmitoleate (SCD3) (**Fig. 1A**). To generate the liver transgenic mice, the cDNA sequences of the transgenes were cloned into the pLiv.LE6 vector construct in which liver-specific expression is achieved by using elements of the human *APOE* gene, including the

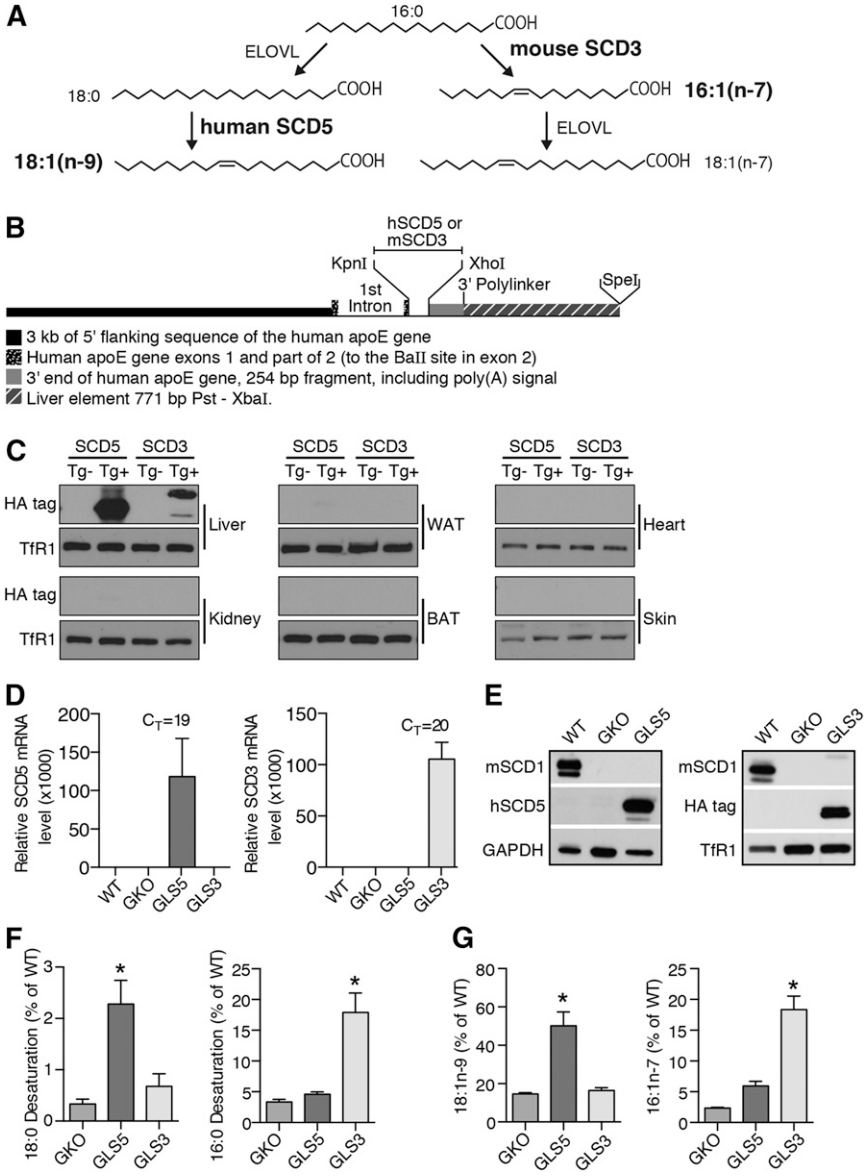

Fig. 1. Generation and characterization of SCD5 and SCD3 liver-specific transgenic mice. A: MUFAs, oleate (18:1n-9) and palmitoleate (16:1n-7), are synthesized by human SCD5 and mouse SCD3, respectively, from saturated fatty acid precursors. B: Construct design for the generation of human *SCD5* and mouse *Scd3* transgenes (Tg) driven by the human *APOE* gene promoter. C: Immunoblot analysis of hemagglutinin-tagged SCD5 and SCD3 microsomal protein in liver, kidney, WAT, brown adipose tissue (BAT), heart, and skin tissue in chow-fed SCD5Tg−, SCD5Tg+, SCD3Tg−, and SCD3Tg+ mice in C57BL/6 background. Transferrin receptor 1 (TfR1) was used as loading control. D–G: Ten-week-old male mice were fed a LD for 10 days (n = 5–6/group) and fasted for 4 h prior to tissue collection. D: Relative mRNA levels of *SCD5* and *Scd3* in liver tissue. The mean cycle threshold value for the transgenic group for each gene is indicated. E: Immunoblot analysis of mouse SCD1 and transgenic protein expression in liver microsomes of WT, GKO, GLS5, and GLS3 mice. TfR1 and GAPDH used as loading controls. F: SCD activity in liver microsomes assessed by desaturation of ^{3}H-(9,10)-stearoyl-CoA (18:0) and ^{3}H-(9,10)-palmitoyl-CoA (16:0). Data are presented as mean percentage of WT activity level for each substrate. G: Relative total (sum of levels in TG, CE, FFA, and GP fractions as reported in supplementary Tables 1–4) hepatic 18:1n-9 and 16:1n-7 levels measured by GLC. Data are presented as percentage of WT fatty acid level. Values are mean ± SEM, $^{*}P < 0.05$ versus GKO; one-way ANOVA analysis with Tukey's post hoc test.

promoter, exons 1 and 2, and the liver control element (20) (Fig. 1B). As expected, expression of the transgenes was robust in liver tissue with minimal to no protein expression detected in a panel of extrahepatic tissues (Fig. 1C). SCD5 and SCD3 transgenic mice in the C57BL/6 genetic background were then crossed into the GKO background that lacks *Scd1* expression in all tissues producing GKO liver-specific SCD5 (GLS5) and GKO liver-specific SCD3 (GLS3) transgenic mice. Quantitative PCR and Western blot analysis revealed that transgenic mice retained high levels of hepatic transgenic gene (Fig. 1D) and protein (Fig. 1E) expression but lacked detectable levels

of SCD1 protein in liver microsomes (Fig. 1E). Like GKO and SCD1 skin-specific knockout mice (26), GLS5 and GLS3 mice exhibited alopecia, closed eye fissures, and dry skin (supplementary Fig. 1) and were visibly indistinguishable from GKO mice at weaning and throughout adulthood, indicating that these phenotypes are not rescued by restoration of liver MUFA synthesis.

We used a modified high-carbohydrate diet (high in sucrose) that supplied 2.5% kcal from fat, hereafter referred to as the LD, to potently induce DNL (16). WT, GKO, GLS5, and GLS3 mice were fed the LD for 10 days. First, changes in SCD activity and hepatic MUFA levels conferred by the expression of *SCD5* or *Scd3* were assessed. Desaturation of ^{3}H-stearoyl-CoA (18:0) was 7-fold higher in GLS5 mice as compared with GKO mice, but not changed in GLS3 mice (Fig. 1F). In contrast, desaturation of ^{3}H-palmitoyl-CoA (16:0) was 5-fold higher in GLS3 mice compared with GKO mice, but unchanged in GLS5 mice (Fig. 1F). These activity assay results confirmed substrate specificities in vivo of the human SCD5 and mouse SCD3 isoforms, in which SCD5 selectively desaturates 18:0 to 18:1n-9 and SCD3 selectively desaturates 16:0 to 16:1n-7. As expected, and in accordance with the SCD activity assays, gas chromatographic analysis of fatty acids in hepatic lipids (summed values in TG, CE, FFA, and GP fractions; reported in supplementary Tables 1–4) revealed 18:1n-9 was significantly increased only in GLS5 mice and 16:1n-7 was increased only in GLS3 mice, relative to GKO mice (Fig. 1G).

Body weight and adiposity phenotypes are restored in GLS5 mice fed a LD

When fed a chow diet, body weight of male mice did not differ, with the exception of GLS5, which was lower than WT mice (supplementary Fig. 2A). Adipose and liver weights and liver and plasma TGs did not differ among GLS5, GLS3, and GKO mice (supplementary Fig. 2B–E).

To assess potential changes in the lipogenic capacity, we measured body weight and adipose tissue weights of WT, GKO, GLS5, and GLS3 male mice fed the LD for 10 days. There were no significant differences in body weight at the start of the study (supplementary Fig. 3). Consistent with our previous results (27), LD-fed GKO mice lost a significant amount of body weight over the 10 day period, with an average loss of nearly 20% of their initial body weight. However, male GLS5 mice lost only 8.6% of the initial body weight. In contrast, GLS3 mice lost nearly double that with an average loss of 16.5%, which was not significantly different from GKO mice. At the end of the feeding period, the body weight of GLS5 mice was significantly greater than that of GKO mice (**Fig. 2A**) and was not different from WT mice. Body weight of GLS3 and GKO mice did not differ and both were significantly lighter than WT mice (Fig. 2A).

Subcutaneous and gonadal WAT depot weights were significantly reduced in GKO mice relative to WT mice. Both adipose tissue depots were significantly increased in weight in GLS5 and GLS3 mice relative to GKO mice (Fig. 2B). However, while the weight of the gonadal adipose depot was partially restored in both GLS5 and GLS3 mice, the subcutaneous depot was fully restored to WT level only in GLS5 mice (Fig. 2B).

GLS5 mice ate significantly more food over the course of the 10 day feeding study as compared with GKO and WT mice (Fig. 2C). Total food intake was increased by 32% in GLS5 mice relative to the WT counterparts. However, when expressed relative to final body weight, the GKO, GLS5, and GLS3 groups ate significantly more food than WT mice (data not shown). Although GLS5 mice consumed more food than GKO mice, plasma leptin was not different between these groups and was significantly lower in GKO, GLS5, and GLS3 mice relative to the WT level (Fig. 2D).

To determine whether circulating FGF21 is influenced by hepatic MUFA levels and could perhaps explain the differential body weight and adiposity phenotypes among the LD-fed mice, we measured plasma FGF21 levels by ELISA. FGF21 was significantly increased in GKO mice relative to

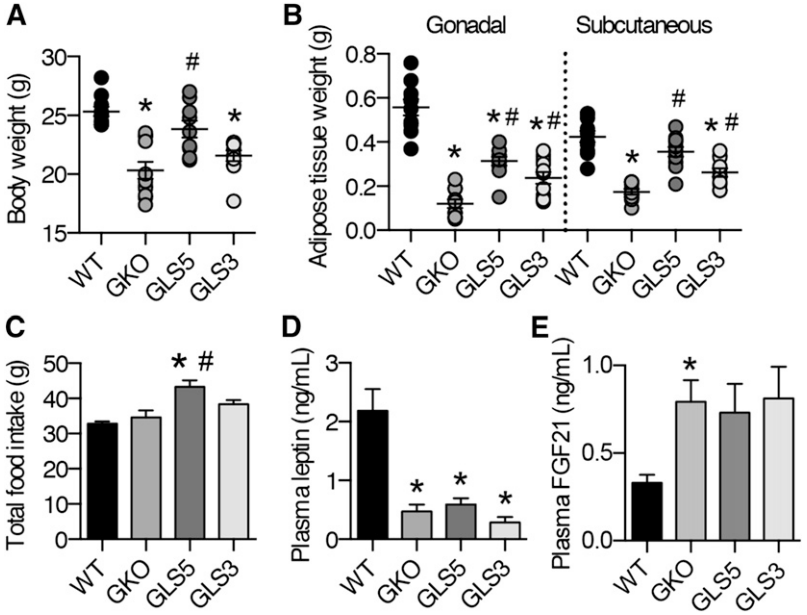

Fig. 2. Body weight and adiposity are rescued in GLS5 mice fed a LD. Male mice (10 weeks old; n = 4–6/group) were fed a LD for 10 days. Food was measured at the start and end of the feeding study. Body weight (A) andgonadal and subcutaneous WAT weight (B) were measured at the end of the 10 day feeding study. C: Total food intake was determined. D: Four hour fasted plasma leptin values were measured using ELISA (n = 6–7/group). E: Plasma FGF21 values were measured using ELISA from 4 h-fasted mice. Values are mean ± SEM. $^{*}P < 0.05$ versus WT, $^{\#}P < 0.05$ versus GKO; one-way ANOVA analysis with Tukey's post hoc test.

WT mice, and was also increased, but only trended toward significance, in GLS5 mice ($P = 0.07$) and GLS3 mice ($P < 0.06$) mice (Fig. 2E). These results suggest that although plasma FGF21 is generally increased by whole-body SCD1 deficiency, it is not likely to be the factor regulating the differential body weight and adiposity responses among the GKO, GLS5, and GLS3 mice.

The differences in GLS5 and GLS3 are consistent with a model where the phenotypes of GKO mice are driven by attenuated oleate production. Overall, these results suggest a role for de novo synthesized hepatic oleate in the regulation of adiposity and body weight under LD conditions, but little effect of palmitoleate.

Blood glucose is increased in GLS5 mice fed a LD

In the absence of SCD1, LD-fed mice are unable to maintain blood glucose levels and become severely hypoglycemic (27). In addition, pyruvate tolerance tests suggest that LD-fed SCD1 LKO mice are unable to synthesize glucose, but this defect in gluconeogenesis is corrected by dietary oleate provided at a level of 20% (w/w) (16). These data suggest that MUFA availability plays a role in the regulation of blood glucose levels. To investigate this further, we measured blood glucose levels in 4 h-fasted male mice fed the LD for 10 days. Blood glucose was significantly increased in GLS5 mice compared with GKO mice (**Fig. 3A**). In contrast, hepatic palmitoleate synthesis in GLS3 mice did not alter blood glucose relative to GKO mice (Fig. 3A). Although fasted blood glucose was significantly elevated in GLS5 mice, the relative hepatic mRNA levels of the gluconeogenic genes *Pck1* and *G6pc* were not significantly different among GKO, GLS5, and GLS3 mice (Fig. 3B). Plasma insulin levels were significantly lower in GKO, GLS5, and GLS3 mice compared with WT mice (Fig. 3C). GKO mice are highly insulin sensitive and glucose tolerant, as previously reported (15, 28). Despite greater adiposity and increased fasted blood glucose levels in GLS5 mice, glucose clearance was not significantly different from GKO or GLS3 mice at any time point during a glucose tolerance test (Fig. 3D), and area under the curve above baseline levels was significantly smaller for all three genotypes as compared with WT mice. Overall, these data suggest that hepatic oleate, at the level produced in GLS5 mice, modestly influences blood glucose regulation.

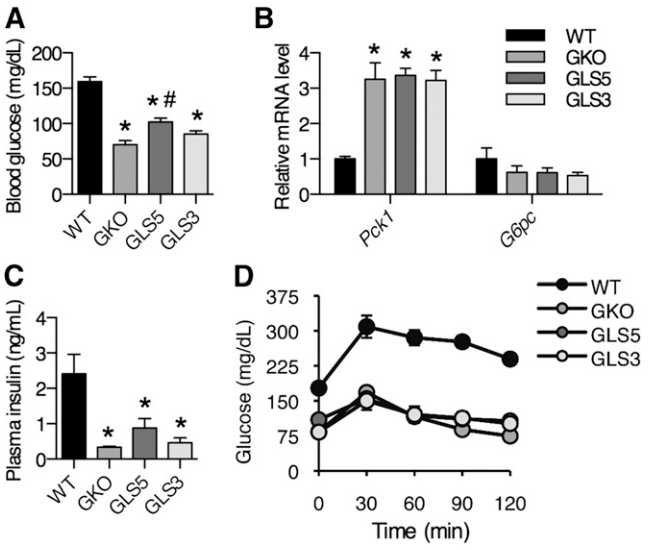

Fig. 3. Blood glucose is increased in GLS5 mice fed a LD. Male mice (10 weeks old) were fed a LD for 10 days. A, C: Blood was collected retro-orbitally from 4 h-fasted mice (n = 4–6/group). A: Glucose was determined using an enzymatic colorimetric assay. B: Relative hepatic mRNA levels of gluconeogenic genes *Pck1* and *G6pc* were measured. C: Plasma insulin levels were measured using ELISA in samples collected as described for (A). D: Glucose tolerance tests were performed in 4 h-fasted male mice. Mice were intraperitoneally injected with 2 g/kg body weight glucose and blood glucose was measured using a glucometer at 0, 30, 60, 90, and 120 min postinjection. Values are mean ± SEM. $^{*}P < 0.05$ versus WT, $^{\#}P < 0.05$ versus GKO; one-way ANOVA analysis with Tukey's post hoc test.

Hepatic lipids accumulate in GLS5 mice during lipogenic dietary conditions

Because GKO and LKO mice display protection against high-carbohydrate diet-induced hepatic steatosis, we questioned whether this protection would be lost with an increase in MUFA availability through the local hepatic synthesis of either oleate or palmitoleate. Biochemical measurement of hepatic TG revealed that GKO mice were protected from lipid accumulation, but GLS5 mice were not (**Fig. 4A**), and accumulated TGs to the same level as WT mice. Hepatic TG level in GLS3 mice was not significantly different from that of GKO mice (Fig. 4A). We also assessed hepatic lipid burden in males by staining neutral lipids in liver tissue sections with oil red O. This histological assessment confirmed the biochemical assay results and demonstrated that while lipid droplets accumulated in GLS5 liver, there was minimal to no accumulation in GKO and GLS3 mice (Fig. 4B). These results reveal that hepatic oleate synthesis is sufficient to rescue the lipid accumulation phenotype of GKO mice during lipogenic dietary conditions, but palmitoleate does not have an effect.

Using GLC, qualitative and quantitative fatty acid analyses of hepatic TG, CE, and GP lipid fractions and nonesterified fatty acids were performed. The mean sum of the fatty acids in each fraction is reported for each genotype (Fig. 4C–F). The sum of fatty acids in the TG fraction further confirmed high levels of hepatic TGs in GLS5 mice and lower levels in GKO and GLS3 mice (Fig. 4C). CEs did not accumulate in the liver of GLS5 mice (Fig. 4D). This suggests that neutral lipid accumulation observed by oil red O in GLS5 mice was due to TGs and not CEs. There were no significant changes in total liver GP levels among the four genotypes (Fig. 4E). FFAs were significantly elevated in GLS5 mice compared with GKO mice and significantly lower in GLS3 mice compared with WT mice (Fig. 4F). Despite increased hepatic FFAs in GLS5 mice, plasma total FFA levels did not differ between groups (data not shown).

Hepatic oleate, but not palmitoleate, positively correlates with adiposity and liver TGs

The results of the hepatic TG measurements suggested that hepatic oleate, but not palmitoleate, may partially explain variation in hepatic TG accumulation during lipogenic

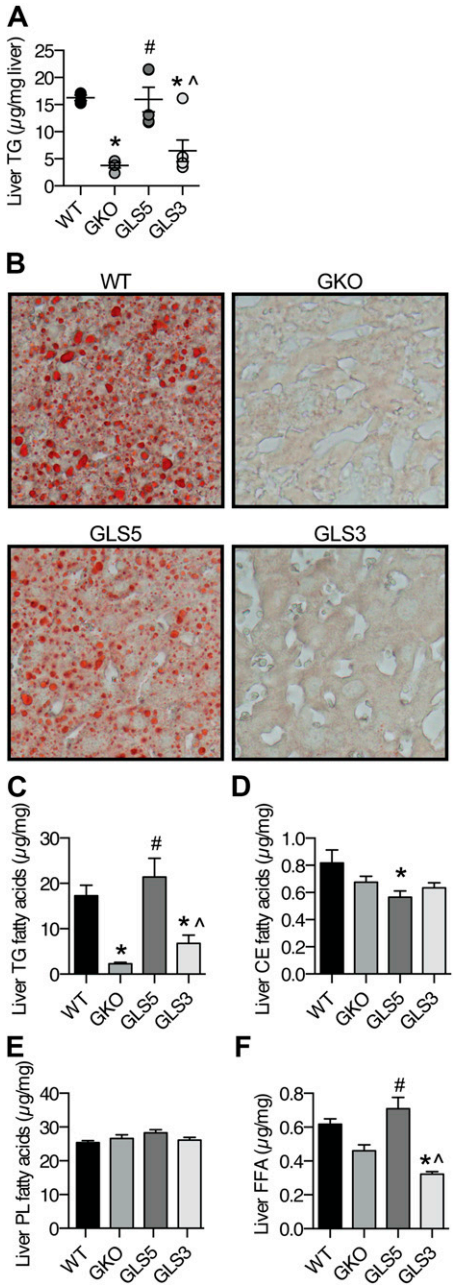

Fig. 4. Hepatic lipid accumulation is restored in male GLS5 mice. Male mice (10 weeks old) were fed a LD for 10 days and 4 h fasted prior to tissue collection (n = 4–6/group). A: Hepatic TGs were extracted from liver tissue and mass was determined by biochemical assay. B:) Liver sections from WT, GKO, GLS5, and GLS3 mice were formalin fixed, cryo-sectioned, and neutral lipids were stained with oil red O and imaged with a 40× objective. C–F: GLC was used to measure total fatty acids in hepatic lipid fractions of TGs (C), CEs (D), GPs (E), and FFAs (F). Values are mean ± SEM. $^{*}P < 0.05$ versus WT, $^{\#}P < 0.05$ versus GKO, $^{\wedge}P < 0.05$ versus GLS5; one-way ANOVA analysis with Tukey's post hoc test.

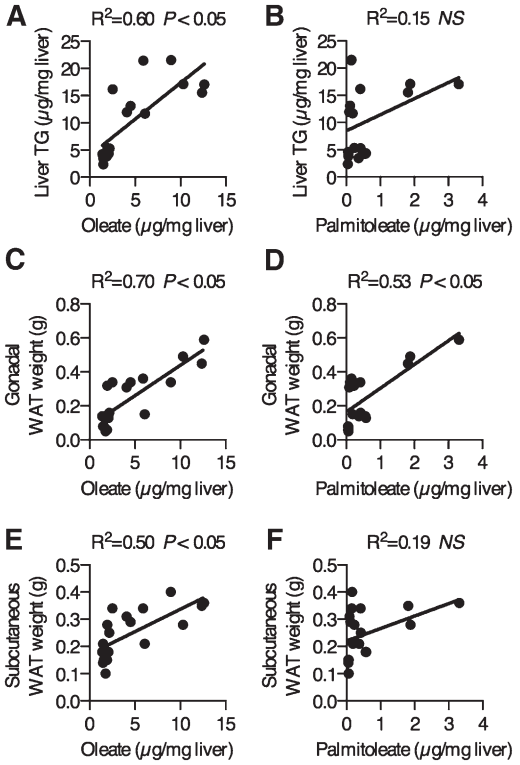

Fig. 5. Hepatic oleate mass correlates with liver TGs and adiposity. Total hepatic oleate and palmitoleate concentrations in WT, GKO, GLS5, and GLS3 male mice fed a LD for 10 days were measured by GLC. Hepatic oleate significantly correlates with liver TG accumulation (A) while total hepatic palmitoleate mass does not correlate with liver TGs (B). Total hepatic oleate levels strongly correlated with gonadal WAT (C) and total hepatic palmitoleate correlated with gonadal WAT (D). Hepatic oleate correlated with subcutaneous WAT weights (E), but total hepatic palmitoleate did not correlate with subcutaneous WAT (F). Data were analyzed using linear regression analysis, n = 19.

dietary conditions. We measured total hepatic oleate and palmitoleate in WT, GKO, GLS5, and GLS3 mice using GLC. Linear regression analyses of all animals revealed that total hepatic oleate levels significantly and directly correlated with hepatic TGs (R^2 = 0.60, **Fig. 5A**), while there was no significant relationship between total hepatic palmitoleate and hepatic TGs (R^2 = 0.15, Fig. 5B). Hepatic oleate (R^2 = 0.70, Fig. 5C) and hepatic palmitoleate (R^2 = 0.53, Fig. 5D) positively correlated with gonadal WAT weight. However, the correlation with hepatic palmitoleate was less robust and the WT group explained the relationship, as the removal of this group from the analysis resulted in complete loss of the correlation (R^2 = 0.007), while the correlation between oleate and gonadal WAT remained significant even without the WT group. Hepatic oleate significantly correlated with the subcutaneous WAT depot (R^2 = 0.50, Fig. 5E) but palmitoleate did not (R^2 = 0.19, Fig. 5F). Taken together, these data suggest that the de novo synthesis of oleate, as compared with that of palmitoleate, is more potent in the positive regulation of lipid accumulation in the liver and WAT in mice on a LD. Furthermore, data from the GLS5 group suggest that when hepatic MUFAs are limited, even a modest increase in hepatic oleate availability is sufficient to induce a shift toward susceptibility to hepatic steatosis and increased adiposity.

Hepatic de novo fatty acid synthesis is not restored in GLS5 or GLS3 mice fed a LD

Next we asked whether hepatic TG accumulation in response to LD in GLS5 mice was due to restoration of hepatic DNL. To address this question, we fed 12–15-week-old

male mice the LD diet for 10 days, performed intraperitoneal injections of ^{3}H-H_2O, and collected tissues 1 h later to measure ^{3}H incorporation into de novo synthesized fatty acids and sterols. As would be predicted from the liver lipid analysis, GKO and GLS3 mice exhibited significantly reduced de novo fatty acid synthesis as compared with the WT rate (**Fig. 6A**). Surprisingly, fatty acid synthesis in GLS5 mice was also low and did not differ from that of the GKO group (Fig. 6A). Hepatic sterol synthesis was not significantly different among the four genotypes (data not shown). Consistent with the fatty acid synthesis results, linear regression analysis revealed that hepatic fatty acid synthesis was not correlated with liver TGs (Fig. 6B). We also measured relative expression levels of genes in the de novo fatty acid synthesis pathway (*Acaca*, *Fasn*, and *Elovl6*) and consistent with the in vivo experiment, the relative mRNA levels of these genes remained low in GKO, GLS5, and GLS3 mice relative to WT mice, although partially restored in GLS5 mice (Fig. 6C). Taken together, these results indicate that hepatic DNL was not responsible for the restored hepatic lipid accumulation observed in GLS5 mice.

Ex vivo hepatic fatty acid oxidation is not significantly changed in GLS5 or GLS3 mice

In absence of an increase in hepatic DNL, another explanation for hepatic lipid accumulation is a defect in fatty acid oxidation. To probe whether differences in hepatic β-oxidation could in part explain the differential susceptibility to hepatic TG accumulation between the GLS5 and GLS3 transgenic models, we directly assessed hepatic mitochondrial fatty acid oxidation. We performed an ex vivo fatty acid oxidation experiment and incubated liver homogenates with ^{14}C-palmitate and measured ^{14}C-labeled CO_2 and ASMs 1 h later. Total hepatic fatty acid oxidation was not different and there were no differences in CO_2 or ASMs (data not shown), even though relative mRNA levels of hepatic fatty acid oxidation-related genes (*Cpt1α*, *Acadm*, and *Acadl)* revealed increased expression of all genes measured in GKO and GLS3 mice, while only *Cpt1α* was increased in GLS5 mice relative to WT mice (Fig. 6D). Regression analysis indicated that differences in liver TG accumulation are not explained by hepatic fatty acid oxidation (R^2 = 0.07, Fig. 6E). Taken together these results show that TG accumulation is not associated with a defect in fatty acid oxidation.

Liver MUFA synthesis influences plasma and WAT MUFA composition

GKO mice are protected from LD-induced hypertriglyceridemia and we questioned whether liver-restored SCD transgenic mice would lose this protection. Plasma TGs were partially restored in GLS5 and GLS3 mice, with an intermediate level between that of GKO and WT mice (Fig. 6F). These data may suggest that altered hepatic MUFA production leads to changes in circulating lipids.

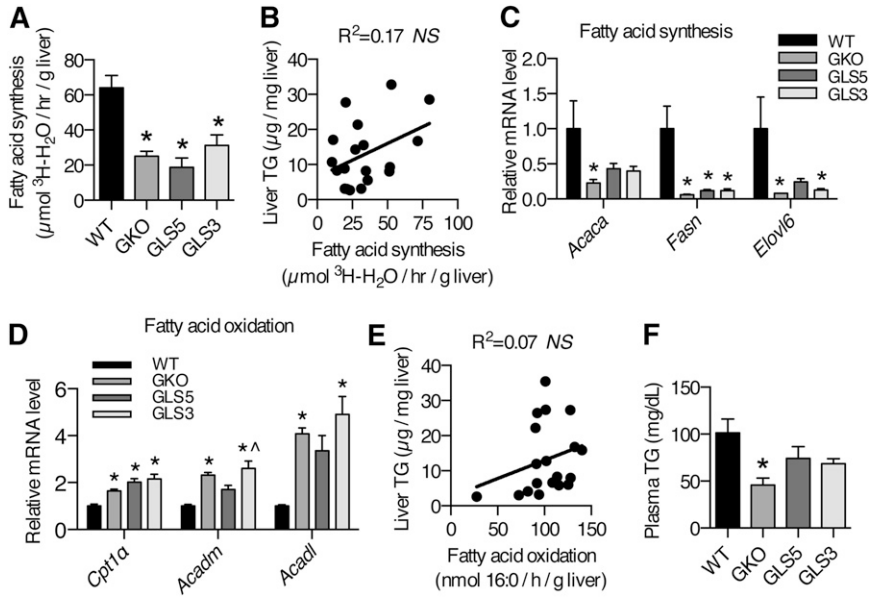

Fig. 6. Hepatic DNL and fatty acid oxidation are not changed in GLS5 and GLS3 mice fed a LD. (A) Hepatic DNL in adult male mice (12–15 weeks old) fed a LD for 10 days. Mice were fasted for 2 h and injected intraperitoneally with 50 mCi ^{3}H-H_2O and tissues were collected 1 h postinjection. Lipids were saponified and separated by TLC (n = 4–6/group). De novo fatty acid synthesis was determined by measuring ^{3}H incorporation into fatty acids by liquid scintillation. B: Hepatic de novo fatty acid synthesis was not significantly correlated with liver TG mass (n = 19). C: Relative expression levels of genes encoding for enzymes involved in de novo fatty acid synthesis were measured in the livers of 4 h-fasted 10-day-old LD-fed male mice. D: Fatty acid oxidation genes were measured in the livers of 4 h-fasted 10-day-old LD-fed male mice (n = 4–6/group). E: Hepatic fatty acid oxidation was not correlated with liver TGs (n = 19). F: Plasma TGs were measured in 4 h-fasted mice fed the LD for 10 days (n = 4–6/group). Values are mean ± SEM. *$P < 0.05$ versus WT, ^$P < 0.05$ versus GLS5; one-way ANOVA analysis with Tukey's post hoc test (A, C, D, F) and linear regression analysis (B, E).

Next we tested whether hepatic de novo synthesized oleate and palmitoleate influence plasma and WAT lipid composition. The secretion of TG-rich VLDL particles from the liver and subsequent lipolysis and fatty acid uptake by peripheral tissues is the primary mechanism by which hepatically derived lipids can influence lipid metabolism and fatty acid composition of extrahepatic tissues. We first analyzed the fatty acid composition of TG, CE, FFA, and GP lipid fractions in liver tissue. Hepatic oleate was significantly increased in TG and GP species in GLS5 mice relative to GKO mice (**Fig. 7A**), while palmitoleate was significantly increased in TG, CE, and GP fractions in GLS3 mice compared with GKO mice (Fig. 7A). The absolute mass of oleate in GLS5 mice was greater than the absolute mass of palmitoleate in GLS3 mice in every lipid fraction analyzed. We predicted that the hepatic MUFA composition would be reflected in circulating lipid species in plasma. Indeed, oleate was significantly increased by 2.5-fold in plasma TGs in GLS5 mice relative to GKO mice (Fig. 7B). Palmitoleate in the TG fraction was more dramatically changed, as it was increased in the GLS3 mice by more than 17 times the level measured in GKO mice (Fig. 7B). Oleate and palmitoleate were also significantly increased as percent of total fatty acids in plasma TGs in GLS5 and GLS3 mice, respectively (supplementary Table 6). Oleate was not significantly changed in any other plasma lipid class in GLS5 mice, although it was significantly reduced in GPs of GLS3 mice (Fig. 7B). Palmitoleate was significantly increased in plasma GPs of GLS3 mice as compared with GKO mice, but not altered in any fraction in GLS5 mice (Fig. 7B). These results show that changes in hepatic MUFA synthesis influence the composition of circulating lipids.

The fatty acids contained in circulating VLDL particles that are taken up by adipose tissue are reesterified into TG molecules, which are the major lipid species of adipose tissue. In the TG fraction of gonadal adipose tissue, we detected significantly elevated oleate in GLS5 mice and significantly elevated palmitoleate in GLS3 mice (Fig. 7C). These data show that hepatic MUFA production influences lipid composition of adipose tissue stores. See supplementary Tables 1–9 in the supplementary information

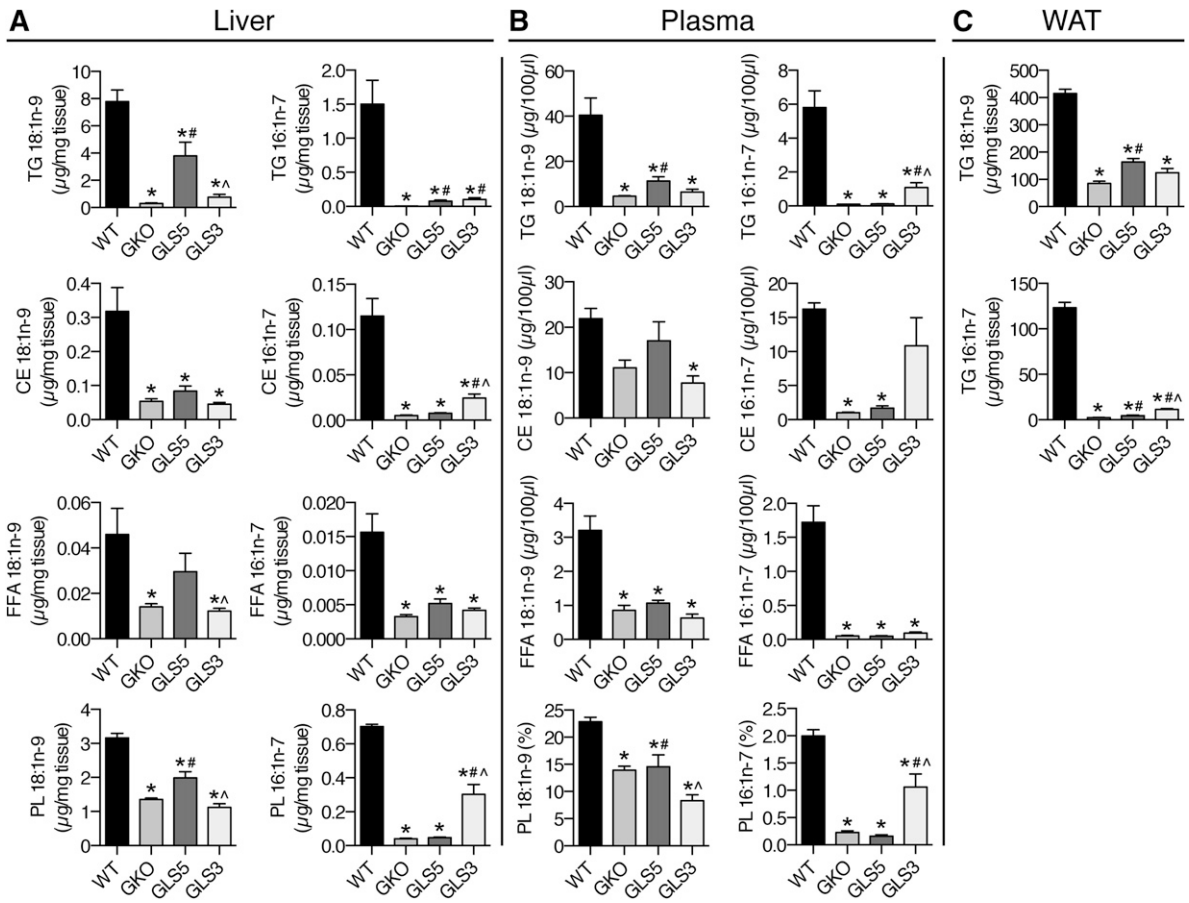

Fig. 7. Hepatic MUFA synthesis influences plasma and gonadal WAT fatty acid composition. Ten-week-old male WT, GKO, GLS5, and GLS3 mice were fed a LD for 10 days (n = 4–6/group) and fasted 4 h prior to tissue collection. GLC was used to analyze oleate (18:1n-9) and palmitoleate (16:1n-7) fatty acid composition of liver (A), plasma (B), and gonadal WAT (C) lipids. Total lipids were extracted from tissues, lipid classes were separated by TLC and TG, CE, FFA, and GP fractions were analyzed in the liver and plasma, and TG was analyzed in gonadal WAT. All data are presented on a fatty acid concentration basis as micrograms per milligram of tissue or micrograms per 100 μl plasma with the exception of plasma GP data, which are expressed as percent of total fatty acids. See supplementary information for complete fatty acid analysis results of these tissues. Values are mean ± SEM. $*P < 0.05$ versus WT, $^{\#}P < 0.05$ versus GKO, $\wedge P < 0.05$ versus GLS5; one-way ANOVA analysis with Tukey's post hoc test.

for detailed fatty acid composition of liver, plasma, and gonadal WAT lipids.

WAT DNL is reduced in GLS5 mice

Differences in adiposity among the SCD models could be explained by differences in WAT DNL and next we assessed in vivo lipid synthesis in the gonadal WAT depot. In this experiment the weight of the gonadal WAT depot was partially restored in both GLS5 and GLS3 mice to a level between that of the WT and GKO groups and the difference between GLS5 and GLS3 adiposity was also significant (**Fig. 8A**). Unexpectedly, the rate of de novo fatty acid synthesis was dramatically and significantly increased in GKO and GLS3 mice despite lower adiposity (Fig. 8B). De novo sterol synthesis followed the same pattern (Fig. 8C). In contrast, GLS5 mice exhibited repressed adipose DNL that was significantly lower than GKO mice, and was not different from WT mice (Fig. 8B, C). Expression of major lipid metabolism regulators, including ChREBP (*Mlxipl*), SREBP-1c (*Srebf1c*), LXRα (*Nr1h3*), and PPARγ were not significantly changed among the genotypes (Fig. 8D). Relative expression of genes encoding enzymes involved in de novo fatty acid (*Fasn* and *Elovl6*) and TG synthesis (*Gpam*, *Dgat1*, and *Dgat2*) largely were also not different among the models, with the exception of *Gpam*, which was elevated in both GLS5 and GLS3 mice (Fig. 8D). There was a trend toward significance of *Dgat2*, with reduced expression in GKO mice. Expression of SREBP2 (*Srebf2*), the major transcriptional regulator of cholesterol synthesis, was not significantly changed, but its target, *Hmgcr*, was significantly increased in GKO relative to WT mice (Fig. 8D), consistent with increased in vivo sterol synthesis. Taken together, the gene expression data suggest that differences in WAT DNL are unlikely to be transcriptionally mediated. Linear regression analyses revealed an inverse relationship between gonadal WAT fatty acid synthesis and liver TGs ($R^2 = 0.26$, Fig. 8E), WAT weight ($R^2 = 0.31$, Fig. 8F), and body weight ($R^2 = 0.39$, Fig. 8G). The decrease in WAT DNL in GLS5 mice and increase in WAT DNL in GKO and GLS3 mice suggests that adipose DNL may be sensitive to changes in hepatic MUFA production.

WAT fatty acid oxidation is reduced in GLS5 mice

Given the differences in adiposity and unexpected DNL results, we next tested to determine whether WAT fatty acid oxidation was different among the models. We performed an ex vivo mitochondrial fatty acid oxidation experiment using gonadal WAT homogenates. Total fatty acid oxidation

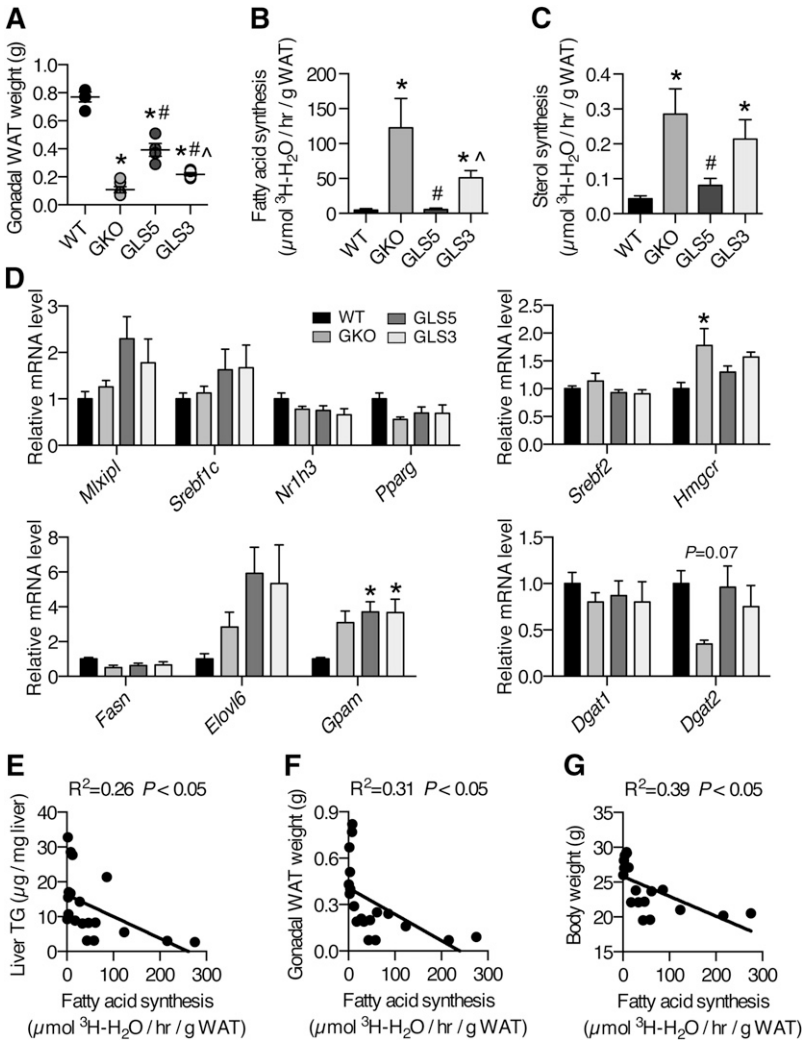

Fig. 8. DNL is repressed in gonadal WAT of GLS5 mice and negatively correlates with lipid accumulation and adiposity. DNL of gonadal WAT (n = 4–6/group) in 12–15-week-old mice. A: Mean gonadal WAT weights. Lipid synthesis was determined by measuring the incorporation of ^3H-H_2O into fatty acids (B) and sterols (C). The experimental procedure and mice are as described in the caption of Fig. 6. D: Relative expression levels of genes encoding for enzymes involved in de novo fatty acid and TG synthesis were measured in gonadal WAT of 4 h-fasted male mice fed a LD for 10 days (n = 5–6/group). E–G: Gonadal WAT fatty acid synthesis was significantly and negatively correlated with liver TG mass ($R^2 = 0.26$) (E), gonadal WAT weight ($R^2 = 0.31$) (F), and body weight ($R^2 = 0.39$) (G), (n = 19). Values are mean ± SEM. $^*P < 0.05$ versus WT, $^{\#}P < 0.05$ versus GKO, $^{\wedge}P < 0.05$ versus GLS5; one-way ANOVA analysis with Tukey's post hoc test (A–D) and linear regression analysis (E–G).

was significantly increased in GKO and GLS3 mice relative to WT mice (**Fig. 9A**). The enhanced fatty acid oxidation of GKO was reversed in the GLS5 mice (Fig. 9A). There was a trend toward increased CO_2 production in GKO and GLS3 mice, but this was not statistically significant (Fig. 9B). Levels of ^{14}C-ASMs were significantly different among the genotypes and followed the same pattern as total fatty acid oxidation (Fig. 9C). We also performed an ex vivo experiment to assess WAT lipolysis. Glycerol release from gonadal WAT was not different among GKO, GLS5, and GLS3 mice, and was elevated in all groups compared with WT mice (Fig. 9D), indicating lipolysis was increased in all three groups. We next measured the genes involved in fatty acid oxidation. There were no significant differences in gonadal WAT gene expression, although the expression patterns of *Acadm* and *Acadl* largely mirrored the trend of the ex vivo fatty acid oxidation results (Fig. 9E). The expression of *Ucp1* was significantly induced in GLS5 mice, while *Ucp2* was significantly induced in GKO mice (Fig. 9E). Regression analysis revealed that adipose tissue fatty acid oxidation and liver TG accumulation are not correlated (Fig. 9F). However, gonadal WAT fatty acid oxidation strongly and negatively correlated with gonadal WAT weight (R^2 = 0.70, Fig. 9G). The negative relationship between WAT fatty acid oxidation and final body weight was also significant, although less robust (R^2 = 0.20, Fig. 9H). These results, taken together with the gonadal WAT DNL results and hepatic lipid data, suggest that hepatic de novo synthesized oleate influences hepatic TG accumulation and adiposity, and is associated with adipose DNL and tissue fatty acid oxidation (**Fig. 10**).

DISCUSSION

This study follows-up on past work describing the role of hepatic SCD1 in mediating the metabolic effects of a LD

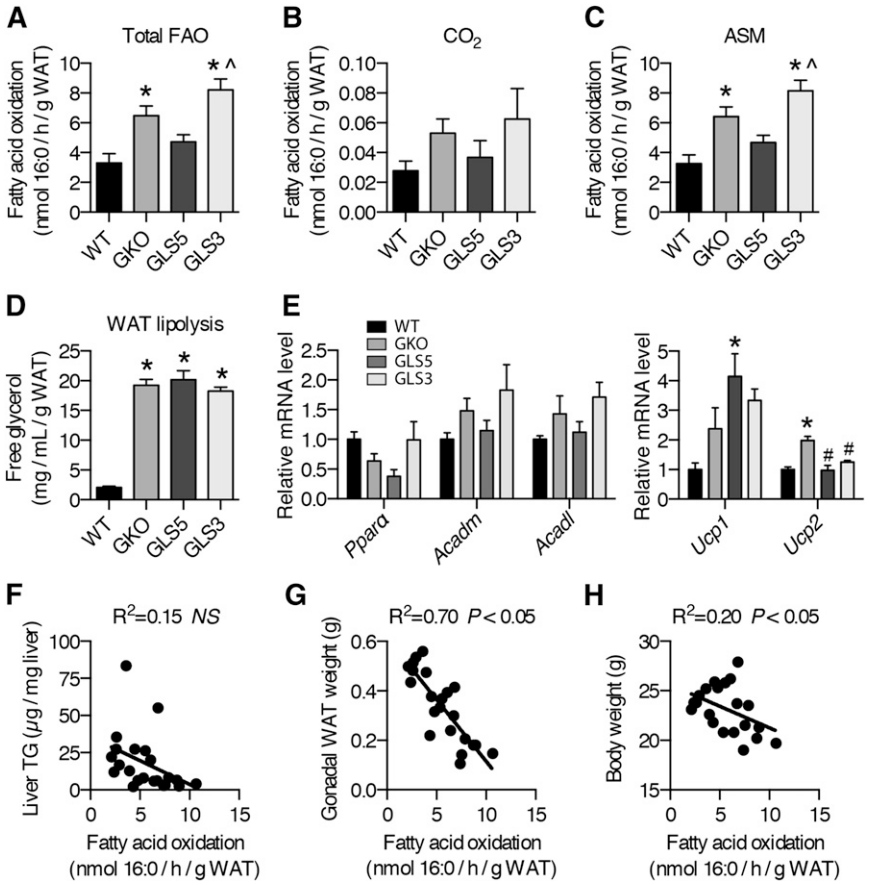

Fig. 9. Fatty acid oxidation in gonadal WAT is repressed in GLS5 mice. Male mice (10–16 weeks old) were fed a LD for 10 days. Mice were fasted 4 h prior to tissue collection (n = 5–6/group). Palmitate (300 μM) with 0.4 μCi 1-^{14}C-palmitate was incubated with WAT homogenates for 1 h. A: Total fatty acid oxidation in gonadal WAT represents the sum of nanomoles of palmitate oxidized to CO_2 and ASMs. Fatty acid oxidation was assessed and ^{14}C-enriched CO_2 (B) and ASM (C) levels were measured using liquid scintillation. D: Free glycerol was measured in gonadal WAT of male mice (n = 6–9/group). E: Relative mRNA levels of fatty acid oxidation-related and uncoupling genes were measured in gonadal WAT of 4 h-fasted 10-day-old LD-fed male mice (n = 5–6/group). F: WAT fatty acid oxidation was not correlated with liver TG accumulation (n = 22). WAT fatty acid oxidation was highly and negatively correlated (R^2 = 0.70) with gonadal WAT weight (G) and WAT fatty acid oxidation was negatively correlated with body weight (R^2 = 0.20) (H) (n = 22). Values are mean ± SEM. *P < 0.05 versus WT, ^P < 0.05 versus GLS5; one-way ANOVA analysis with Tukey's post hoc test (A–E) and linear regression analysis (F–H).

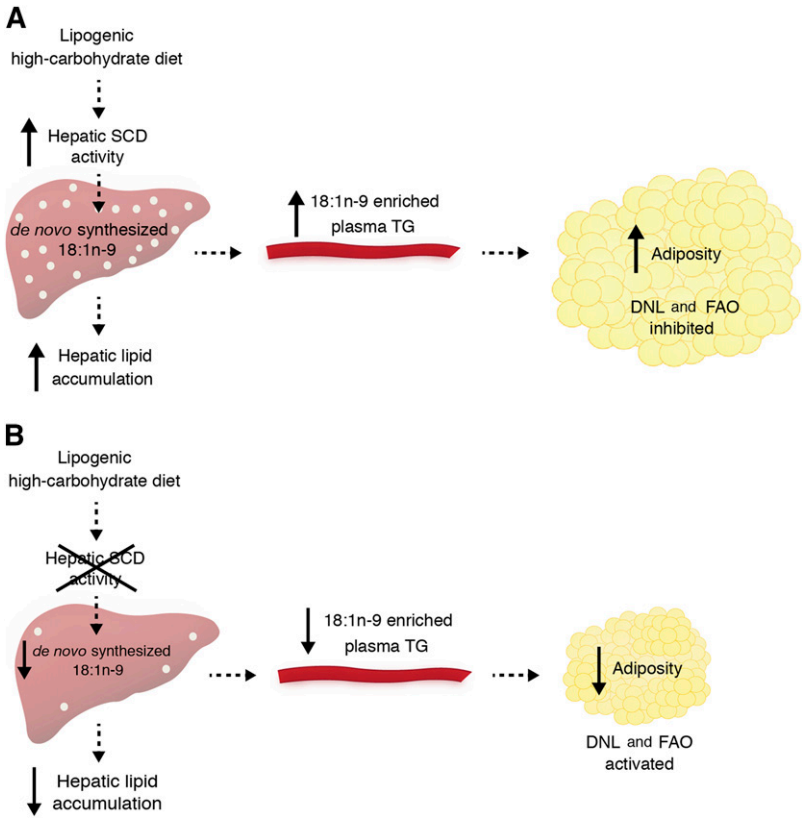

Fig. 10. Proposed model of the metabolic effects of de novo-synthesized hepatic 18:1n-9 within the context of a LD. A: A lipogenic high-carbohydrate diet stimulates hepatic SCD activity, causing an increase in the de novo synthesis of 18:1n-9 and subsequent hepatic TG accumulation. Hepatic 18:1n-9 becomes available to peripheral tissues through circulating 18:1n-9-containing TG-rich VLDL particles. In gonadal WAT, there is a net effect of increased adiposity and the hepatically derived 18:1n-9 is associated with repression of the DNL and fatty acid oxidation (FAO) pathways. B: However, when hepatic SCD activity is reduced, there is a reduction in de novo-synthesized hepatic 18:1n-9 and a LD fails to induce hepatic lipid accumulation. Plasma TG 18:1n-9 content and peripheral tissue 18:1n-9 uptake are both reduced with a net effect of reduced adiposity. With decreased 18:1n-9, fatty acid synthesis and oxidation pathways are activated.

(16, 27). Some phenotypes of GKO mice are recapitulated in LKO mice, such as protection from LD-induced liver steatosis and adipose tissue lipid accumulation (16). The focus of this study was to determine which product of hepatic SCD activity drives the phenotypes of increased lipid accumulation in liver and adipose tissue. We developed two novel mouse models where either oleate or palmitoleate production was restored in the liver in the GKO background. We show that restoring liver synthesis of oleate, but not palmitoleate, rescues adaptation to LD feeding in GKO mice, blocking the prevention of ectopic lipid accumulation. Furthermore total hepatic oleate strongly correlated with total hepatic TG accumulation and with adipose tissue mass, whereas total hepatic palmitoleate did not. These experiments show that a modest change in hepatic oleate synthesis can have dramatic whole-body metabolic effects.

At the outset of the study, we hypothesized that reduced hepatic de novo fatty acid synthesis accounted for the protection against lipid accumulation in LKO mice on the LD. However, data shown here demonstrate that despite increased hepatic oleate availability at the level produced in the liver of GLS5 mice, hepatic de novo fatty acid synthesis is not enhanced, indicating that the lipid accumulation is not driven by increased lipid synthesis. Our data also eliminate deficient hepatic fatty acid oxidation as the underlying cause of the steatosis phenotype, as there were no significant differences in hepatic β-oxidation among the GKO, GLS5, and GLS3 models. An alternate possible explanation for increased lipid stores in the liver of GLS5 mice is based on studies of substrate preference of DGAT2. DGAT2 synthesizes TGs from diacylglycerol and prefers de novo synthesized fatty acids to fatty acids supplied in the diet (29, 30), and competition assays suggest that DGAT2 prefers oleate (31, 32). In this case, restoration of oleate could enhance flux through DGAT2. The proximity of SCD and DGAT2 in the endoplasmic reticulum membrane ensures channeling of de novo synthesized MUFAs for esterification due to local enrichment at the endoplasmic reticulum membrane. This could explain how the modest restoration of stearate desaturation in the GLS5 mice is sufficient to drive a 40% enrichment in oleate in liver fatty acid composition and an increase in total TG accumulation.

Relative to GKO mice, GLS5 restored liver steatosis and expanded the adipose tissue mass. This suggests that liver MUFA synthesis may be involved in the regulation of lipid homeostasis outside of the liver. Although changes in liver MUFA composition of the transgenic models were reflected in the plasma TG fatty acid composition, plasma lipid load may drive the adiposity phenotypes in the GKO and transgenic models, in which plasma TG and adipose tissue weights were low in GKO mice and intermediate in GLS5 and GLS3 mice. An alternate explanation is that lipid fatty acid composition influences the metabolic response in adipose tissue.

In analyzing lipid metabolism in expanded and nonresponsive adipose tissue, we unexpectedly determined that the two models with the lowest adipose tissue mass had the highest rates of DNL, with fatty acid synthesis 25- and 10-fold higher in the WAT of GKO and GLS3 mice, respectively, as compared with WT mice. These results demonstrate that increased WAT mass is not predictive of increased DNL and that increases in DNL do not necessarily

direct increased adiposity. Regression analyses showed that adipose tissue fatty acid synthesis was negatively correlated with liver TG, gonadal WAT weight, and total body weight. These findings are consistent with the concept that the ability to upregulate WAT DNL is metabolically beneficial in the context of a LD. In clinical studies, decreased lipogenic gene expression has been reported in obese human subjects, which correlated inversely with markers of insulin resistance and hepatic steatosis (33). Eissing et al. (33) also demonstrated that in subjects who underwent bariatric surgery, increased lipogenic gene expression in WAT was associated with weight loss and improved glucose homeostasis postsurgery. It is not unprecedented for WAT DNL to be increased when liver DNL is low. Independent models of altered lipid metabolism have demonstrated a relationship between liver DNL and WAT DNL, with reduced hepatic DNL accompanied by upregulated adipose DNL, likely as a compensatory response (34, 35).

The apparent incongruity of reduced adiposity with increased DNL in GKO and GLS3 mice is explained in part by an increased rate of fatty acid oxidation. Regression analysis showed a strong negative correlation between fatty acid oxidation in WAT and gonadal adipose tissue weight, explaining up to 70% of the weight variation. This suggests that the oxidation of fatty acids in adipose tissue exerts control over total adiposity. In contrast, regression analysis showed adipose tissue DNL was negatively associated with hepatic lipid accumulation. Taken together these results reveal that lipid storage homeostasis is associated with the metabolic status of adipose tissue.

Potential mechanisms by which hepatic de novo synthesized oleate exerts systemic effects to regulate specific metabolic pathways in WAT remain unknown. One possibility is that oleate itself or a more complex lipid that it is incorporated into exerts transcriptional regulation over genes in the β-oxidation or DNL pathways via regulation of transcription factors. Indeed, fatty acid-mediated regulation of transcription factors has been well-described (36). However, we previously demonstrated that in SCD1 GKO mice the protection from hepatic steatosis and increased adiposity is not meditated through PPARα, a transcription factor that exerts significant control over fatty acid oxidation (37) and the results of the current study do not support a transcriptional mechanism. Another possibility is that oleate or a more complex lipid directly inhibits enzymes in the β-oxidation or DNL pathways. MUFAs have been shown to be required for a number of specific protein interactions that elicit a broad range of biological effects. For example, Liu et al. (38) recently demonstrated that endogenous, but not exogenous, oleate and palmitoleate inhibit the activity of fatty acid amide hydrolase, an enzyme that degrades endocannabinoids, and explains the mechanism through which endocannabinoids decrease insulin sensitivity. Activation of Wnt proteins requires them to first become acylated with palmitoleate (39), while oleate is a required component of specific GP species that activate PPARα in the liver (40) and muscle (41). Perhaps enzymes in the fatty acid oxidation or synthesis pathways distinguish between oleate and palmitoleate and are regulated by the former but not the latter. However, it should also be emphasized that the dramatic metabolic changes in WAT in this study were in SCD1-deficient tissue, as GKO, GLS5, and GLS3 mice were all SCD1 global knockouts. Therefore, the effects of oleate on metabolic regulation should be further tested in adipocytes with WT SCD1 expression.

Recent reports support a role for palmitoleate in maintenance of metabolic health. In mice, Cao et al. (42) showed that circulating palmitoleate synthesized in WAT acts as a lipokine in peripheral tissues, suppressing hepatic lipogenesis and increasing skeletal muscle insulin sensitivity. Parallel independent studies showed that palmitoleate supplementation increases insulin sensitivity (43, 44), although consensus on its effect on hepatic lipid accumulation is lacking. In humans, the role of plasma palmitoleate is less clear. Palmitoleate positively correlates with insulin sensitivity in overweight subjects (45), but the association is not observed in obese adults or children (46, 47). Although hepatic palmitoleate synthesis is restored in GLS3 mice, GKO mice are already dramatically protected against diet-induced metabolic derangements, and further benefits of increased palmitoleate were not observed.

A striking result of the current study was the significant increase in total food intake in LD-fed GLS5 mice as compared with WT mice. With increased adiposity, one could expect plasma leptin levels to be increased in GLS5 mice relative to GKO mice, and that in turn would be predicted to reduce food intake. In this study, plasma leptin in GLS5 mice was reduced compared with WT mice and not different from GKO mice, while food intake was enhanced for GLS5 mice only, separating adiposity and food intake from absolute plasma leptin levels. A potential explanation for the similar body weights in GLS5 and WT mice, despite the increased food intake in GLS5 mice, is an induction of uncoupling. Indeed, we observed significantly induced *Ucp1* expression in WAT of GLS5 mice, which may suggest that energy dissipation is increased in these mice.

The possibility that the absolute mass of oleate is driving the phenotypes in this study cannot be excluded based on the current study. However, it is unlikely that palmitoleate levels would reach oleate levels, as the metabolic fates of these fatty acids are not equivalent and conversion to elongated species is not equivalent. In general, the elongation of the product of SCD5, 18:1n-9, to 20:1n-9 is minimal, and 20:1n-9 accumulates to approximately 2% that of 18:1n-9. In contrast, the elongation of the product of SCD3, 16:1n-7, to 18:1n-7 readily occurs and approximately equal levels of these two n-7 fatty acids are present in the liver. In GLS5 mice, levels of 18:1n-9 were restored to 50% of WT levels, whereas in GLS3 mice, levels of 16:1n-7 reached only 20% of WT levels. Given its metabolic fate, the 20% increase in 16:1n-7 detected in the GLS3 liver likely underestimates the increase in its rate of de novo synthesis.

We have identified a model of lipid metabolism homeostasis involving communication between liver and adipose tissue stores. Importantly, this work reveals that lipid metabolism

and lipid storage homeostasis are both sensitive to hepatic oleate production, where one of the major products of SCD activity can influence the balance of storage and utilization in adipose tissue. However, additional work will be required to understand whether these are direct or indirect effects of hepatic oleate. An understanding of factors that regulate the balance of lipid storage among adipose depots and in hepatic tissue is relevant to human health. The degree of risk for metabolic impairment is dependent on the location of ectopic lipid stores, where fatty liver is associated with poorer outcomes than expanded adipose depots. Our studies suggest that an imbalance in lipid stores may be corrected through interventions targeting SCD activities in liver.

The authors thank Dr. Makoto Miyazaki for design and development of the transgenic mouse lines. They also thank Laura Vanderploeg in the University of Wisconsin-Madison Biochemistry Department Media Center and Mary Cantu for assistance with design and production of figures. They thank Dr. Tom Pugh for assistance with liver histology.

REFERENCES

1. Flegal, K. M., M. D. Carroll, B. K. Kit, and C. L. Ogden. 2012. Prevalence of obesity and trends in the distribution of body mass index among US adults, 1999–2010. *JAMA.* **307:** 491–497.
2. Nguyen, D. M., and H. B. El-Serag. 2010. The epidemiology of obesity. *Gastroenterol. Clin. North Am.* **39:** 1–7.
3. Moore, J. B. 2010. Non-alcoholic fatty liver disease: the hepatic consequence of obesity and the metabolic syndrome. *Proc. Nutr. Soc.* **69:** 211–220.
4. Cohen, J. C., J. D. Horton, and H. H. Hobbs. 2011. Human fatty liver disease: old questions and new insights. *Science.* **332:** 1519–1523.
5. Birkenfeld, A. L., and G. I. Shulman. 2014. Nonalcoholic fatty liver disease, hepatic insulin resistance and type 2 diabetes. *Hepatology.* **59:** 713–723.
6. Aarsland, A., D. Chinkes, and R. Wolfe. 1997. Hepatic and whole-body fat synthesis in humans during carbohydrate overfeeding. *Am. J. Clin. Nutr.* **65:** 1774–1782.
7. Hellerstein, M. K., J. M. Schwarz, and R. A. Neese. 1996. Regulation of hepatic de novo lipogenesis in humans. *Annu. Rev. Nutr.* **16:** 523–557.
8. Stanhope, K. L., J. M. Schwarts, N. L. Keim, S. C. Griffen, A. A. Bremer, J. L. Graham, B. Hatcher, C. L. Cox, A. Dyachenko, W. Zhang, et al. 2009. Consuming fructose-sweetened, not glucose-sweetened, beverages increases visceral adiposity and lipids and decreases insulin sensitivity in overweight/obese humans. *J. Clin. Invest.* **119:** 1322–1334.
9. Vos, M. B., and J. E. Lavine. 2013. Dietary fructose in nonalcoholic fatty liver disease. *Hepatology.* **57:** 2525–2531.
10. Donnelly, K. L., C. I. Smith, S. J. Schwarzenberg, J. Jessurun, M. D. Boldt, and E. J. Parks. 2005. Sources of fatty acids stored in liver and secreted via lipoproteins in patients with nonalcoholic fatty liver disease. *J. Clin. Invest.* **115:** 1343–1351.
11. Lodhi, I. J., X. Wei, and C. F. Semenkovich. 2011. Lipoexpediency: de novo lipogenesis as a metabolic signal transmitter. *Trends Endocrinol. Metab.* **22:** 1–8.
12. Hulver, M. W., J. R. Berggren, M. J. Carper, M. Miyazaki, J. M. Ntambi, E. P. Hoffman, J. P. Thyfault, R. Stevens, G. L. Dohm, J. A. Houmard, et al. 2005. Elevated stearoyl-CoA desaturase-1 expression in skeletal muscle contributes to abnormal fatty acid partitioning in obese humans. *Cell Metab.* **2:** 251–261.
13. Attie, A. D., R. M. Krauss, M. P. Gray-Keller, A. Brownlie, M. Miyazaki, J. J. Kastelein, A. J. Lusis, A. F. Stalenhoef, J. P. Stoehr, M. R. Hayden, et al. 2002. Relationship between stearoyl-CoA desaturase activity and plasma triglycerides in human and mouse hypertriglyceridemia. *J. Lipid Res.* **43:** 1899–1907.
14. Warensjö, E., E. Ingelsson, P. Lundmark, L. Lannfelt, A. C. Syvanen, B. Vessby, and U. Riserus. 2007. Polymorphisms in the SCD1 gene: associations with body fat distribution and insulin sensitivity. *Obesity (Silver Spring).* **15:** 1732–1740.
15. Ntambi, J. M., M. Miyazaki, J. P. Stoehr, H. Lan, C. M. Kendziorski, B. S. Yandell, Y. Song, P. Cohen, J. M. Friedman, and A. D. Attie. 2002. Loss of stearoyl–CoA desaturase-1 function protects mice against adiposity. *Proc. Natl. Acad. Sci. USA.* **99:** 11482–11486.
16. Miyazaki, M., M. T. Flowers, H. Sampath, K. Chu, C. Otzelberger, X. Liu, and J. M. Ntambi. 2007. Hepatic stearoyl-CoA desaturase-1 deficiency protects mice from carbohydrate-induced adiposity and hepatic steatosis. *Cell Metab.* **6:** 484–496.
17. Zheng, Y., S. M. Prouty, A. Harmon, J. P. Sundberg, K. S. Stenn, and S. Parimoo. 2001. Scd3–a novel gene of the stearoyl-CoA desaturase family with restricted expression in skin. *Genomics.* **71:** 182–191.
18. Miyazaki, M., H. J. Kim, W. C. Man, and J. M. Ntambi. 2001. Oleoyl-CoA is the major de novo product of stearoyl-CoA desaturase 1 gene isoform and substrate for the biosynthesis of the Harderian gland 1-alkyl-2,3-diacylglycerol. *J. Biol. Chem.* **276:** 39455–39461.
19. Miyazaki, M., F. E. Gomez, and J. M. Ntambi. 2002. Lack of stearoyl-CoA desaturase-1 function induces a palmitoyl-CoA Delta6 desaturase and represses the stearoyl-CoA desaturase-3 gene in the preputial glands of the mouse. *J. Lipid Res.* **43:** 2146–2154.
20. Simonet, W. S., N. Bucay, S. J. Lauer, and J. M. Taylor. 1993. A far-downstream hepatocyte-specific control region directs expression of the linked human apolipoprotein E and C–I genes in transgenic mice. *J. Biol. Chem.* **268:** 8221–8229.
21. Flowers, M. T., L. Ade, M. S. Strable, and J. M. Ntambi. 2012. Combined deletion of SCD1 from adipose tissue and liver does not protect mice from obesity. *J. Lipid Res.* **53:** 1646–1653.
22. Folch, J., M. Lees, and G. H. S. Stanley. 1957. A simple method for the isolation and purification of total lipides from animal tissues. *J. Biol. Chem.* **226:** 497–509.
23. Koopman, R., G. Schaart, and M. Hesselink. 2001. Optimization of oil red O staining permits combination with immunofluorescence and automated quantification of lipids. *Histochem. Cell Biol.* **116:** 63–68.
24. Jeske, D. J., and J. M. Dietschy. 1980. Regulation of rates of cholesterol synthesis in vivo in the liver and carcass of the rat measured using [3H]water. *J. Lipid Res.* **21:** 364–376.
25. Hirschey, M. D., T. Shimazu, E. Goetzman, E. Jing, B. Schwer, D. B. Lombard, C. A. Grueter, C. Harris, S. Biddinger, O. R. Ilkayeva, et al. 2010. SIRT3 regulates mitochondrial fatty-acid oxidation by reversible enzyme deacetylation. *Nature.* **464:** 121–125.
26. Sampath, H., M. T. Flowers, X. Liu, C. M. Paton, R. Sullivan, K. Chu, M. Zhao, and J. M. Ntambi. 2009. Skin-specific deletion of stearoyl-CoA desaturase-1 alters skin lipid composition and protects mice from high fat diet-induced obesity. *J. Biol. Chem.* **284:** 19961–19973.
27. Flowers, M. T., A. K. Groen, T. A. Oler, M. P. Keller, Y. Choi, K. L. Schueler, O. C. Richards, H. Lan, M. Miyazaki, F. Kuipers, et al. 2006. Cholestasis and hypercholesterolemia in SCD1-deficient mice fed a low-fat, high-carbohydrate diet. *J. Lipid Res.* **47:** 2668–2680.
28. Rahman, S. M., A. Dobrzyn, P. Dobrzyn, S. H. Lee, M. Miyazaki, and J. M. Ntambi. 2003. Stearoyl-CoA desaturase 1 deficiency elevates insulin-signaling components and down-regulates protein-tyrosine phosphatase 1B in muscle. *Proc. Natl. Acad. Sci. USA.* **100:** 11110–11115.
29. Yen, C-L. E., S. J. Stone, S. Koliwad, C. Harris, and R. V. Farese. 2008. Thematic review series: glycerolipids. DGAT enzymes and triacylglycerol biosynthesis. *J. Lipid Res.* **49:** 2283–2301.
30. Wurie, H. R., L. Buckett, and V. A. Zammit. 2012. Diacylglycerol acyltransferase 2 acts upstream of diacylglycerol acyltransferase 1 and utilizes nascent diglycerides and de novo synthesized fatty acids in HepG2 cells. *FEBS J.* **279:** 3033–3047.
31. Man, W. C., M. Miyazaki, K. Chu, and J. Ntambi. 2006. Colocalization of SCD1 and DGAT2: implying preference for endogenous monounsaturated fatty acids in triglyceride synthesis. *J. Lipid Res.* **47:** 1928–1939.
32. Cases, S., S. J. Stone, P. Zhou, E. Yen, B. Tow, K. D. Lardizabel, T. Voelker, and R. V. Farese, Jr. 2001. Cloning of DGAT2, a second mammalian diacylglycerol acyltransferase, and related family members. *J. Biol. Chem.* **276:** 38870–38876.
33. Eissing, L., T. Scherer, K. Todter, U. Knippschild, J. W. Greve, W. A. Buurman, H. O. Pinnschmidt, S. S. Rensen, A. M. Wolf, A. Bartelt, et al. 2013. De novo lipogenesis in human fat and liver is linked to ChREBP-β and metabolic health. *Nat. Commun.* **4:** 1528.
34. Beaven, S. W., A. Matveyenko, K. Wroblewski, L. Chao, D. Wilpitz, T. W. Hsu, J. Lentz, B. Drew, A. L. Hevener, and P. Tontonoz. 2013.

Reciprocal regulation of hepatic and adipose lipogenesis by liver X receptors in obesity and insulin resistance. *Cell Metab.* **18:** 106–117.
35. Kuriyama, H., G. Liang, L. J. Engelking, J. D. Horton, J. L. Goldstein, and M. S. Brown. 2005. Compensatory increase in fatty acid synthesis in adipose tissue of mice with conditional deficiency of SCAP in liver. *Cell Metab.* **1:** 41–51.
36. Jump, D. B., S. Tripathy, and C. M. Depner. 2013. Fatty acid-regulated transcription factors in the liver. *Annu. Rev. Nutr.* **33:** 249–269.
37. Miyazaki, M., A. Dobrzyn, H. Sampath, S. H. Lee, W. C. Man, K. Chu, J. M. Peters, F. J. Gonzales, and J. M. Ntambi. 2004. Reduced adiposity and liver steatosis by stearoyl-CoA desaturase deficiency are independent of peroxisome proliferator-activated receptor-alpha. *J. Biol. Chem.* **279:** 35017–35024.
38. Liu, J., R. Cinar, K. Xiong, G. Godlewski, T. Jourdan, Y. Lin, J. M. Ntambi, and G. Kunos. 2013. Monounsaturated fatty acids generated via stearoyl CoA desaturase-1 are endogenous inhibitors of fatty acid amide hydrolase. *Proc. Natl. Acad. Sci. USA.* **110:** 18832–18837.
39. Rios-Esteves, J., and M. D. Resh. 2013. Stearoyl CoA desaturase is required to produce active, lipid-modified Wnt proteins. *Cell Reports.* **4:** 1072–1081.
40. Chakravarthy, M. V., I. J. Lodhi, L. Yin, R. R. Malapaka, H. E. Xu, J. Turk, and C. F. Semenkovich. 2009. Identification of a physiologically relevant endogenous ligand for PPARalpha in liver. *Cell.* **138:** 476–488.
41. Liu, S., J. D. Brown, K. J. Stanya, E. Homan, M. Leidl, K. Inouye, P. Bhargava, M. R. Gangl, L. Dai, B. Hatano, et al. 2013. A diurnal serum lipid integrates hepatic lipogenesis and peripheral fatty acid use. *Nature.* **502:** 550–554.
42. Cao, H., K. Gerhold, J. R. Mayers, M. M. Wiest, S. M. Watkins, and G. S. Hotamisligil. 2008. Identification of a lipokine, a lipid hormone linking adipose tissue to systemic metabolism. *Cell.* **134:** 933–944.
43. Yang, Z-H., H. Miyahara, and A. Hatanaka. 2011. Chronic administration of palmitoleic acid reduces insulin resistance and hepatic lipid accumulation in KK-Ay Mice with genetic type 2 diabetes. *Lipids Health Dis.* **10:** 120.
44. Guo, X., H. Li, H. Xu, V. Halim, W. Zhang, H. Wang, K. T. Ong, S. L. Woo, R. L. Walzem, D. G. Mashek, et al. 2012. Palmitoleate induces hepatic steatosis but suppresses liver inflammatory response in mice. *PLoS ONE.* **7:** e39286.
45. Arregui, M., B. Buijsse, N. Stefan, D. Corella, E. Fisher, R. di Giuseppe, O. Coltell, S. Knuppel, K. Aleksandrova, H. G. Joost, et al. 2012. Heterogeneity of the stearoyl-CoA desaturase-1 (SCD1) gene and metabolic risk factors in the EPIC-Potsdam study. *PLoS ONE.* **7:** e48338.
46. Fabbrini, E., F. Magkos, X. Su, N. A. Abumrad, N. Nejedly, C. C. Coughlin, A. L. Okunade, B. W. Patterson, and S. Klein. 2011. Insulin sensitivity is not associated with palmitoleate availability in obese humans. *J. Lipid Res.* **52:** 808–812.
47. Okada, T., N. Furuhashi, Y. Kuromori, M. Miyashita, F. Iwata, and K. Harada. 2005. Plasma palmitoleic acid content and obesity in children. *Am. J. Clin. Nutr.* **82:** 747–750.